

論文 / 著書情報  
Article / Book Information

Title	Optical properties of highly crystalline Y2O3:Er,Yb nanoparticles prepared by laser ablation in water
Authors	Takashi Nunokawa, Osamu Odawara, Hiroyuki Wada
Citation	Materials Research Express, vol. 1, ,
Pub. date	2014, 8
Note	This is an author-created, un-copyedited version of an article accepted for publication/published in Materials Research Express. IOP Publishing Ltd is not responsible for any errors or omissions in this version of the manuscript or any version derived from it. The Version of Record is available online at <a href="http://dx.doi.org/10.1088/2053-1591/1/3/035043">http://dx.doi.org/10.1088/2053-1591/1/3/035043</a> .
Note	このファイルは著者（最終）版です。 This file is author (final) version.

**Title:**

Optical properties of highly crystalline  $\text{Y}_2\text{O}_3:\text{Er},\text{Yb}$  nanoparticles prepared by laser ablation in water

**Author names and affiliations:**

Takashi Nunokawa, Osamu Odawara, Hiroyuki Wada

Interdisciplinary Graduate School of Science and Engineering, Tokyo Institute of Technology, 4259 Nagatsuta-cho, Midoriku, Yokohama 226-8502, Japan

**Corresponding author at:**

Takashi Nunokawa

Phone/Fax: +81-45-924-5567

E-mail: [nunokawa.t.aa@m.titech.ac.jp](mailto:nunokawa.t.aa@m.titech.ac.jp)

Postal address: J2-41, 4259 Nagatsuta-cho, Midoriku, Yokohama 226-8502, Japan

## **Abstract**

Y<sub>2</sub>O<sub>3</sub>:Er,Yb nanoparticles were prepared by laser ablation in water. We investigated crystallinity, distribution of dopant, and optical properties of the prepared nanoparticles. The full-width half-maximum (FWHD) of the crystalline peak of nanoparticles measured by an X-ray diffractometer (XRD) barely changed. Further, using scanning transmission electron microscopy–energy dispersive X-ray spectroscopy (STEM–EDX), we confirmed the peaks of Y, Er, Yb, and O. Moreover, on the basis of the optical properties of the nanoparticles, the emission of red ( $^2F_{9/2} \rightarrow ^4I_{15/2}$ ) and green ( $^2H_{11/2}, ^4S_{3/2} \rightarrow ^4I_{15/2}$ ) was confirmed. We also investigated the emission intensity as a function of the excitation power of 980 nm LD in the prepared nanoparticles. The photon avalanche effect was observed at the excitation power of 100 mW. These results confirmed that uniformly Er-Yb-doped Y<sub>2</sub>O<sub>3</sub> nanoparticles were successfully prepared by laser ablation in water.

## **Keywords**

Nanoparticle, Upconversion, Y<sub>2</sub>O<sub>3</sub>, Laser ablation, Nanosecond laser

## **Introduction**

In recent years, rare-earth-doped phosphors have frequently been researched because of their unique optical properties. As potential applications, the functionalization of biomaterials <sup>[1-6]</sup>, solar cells <sup>[7-9]</sup> and white LEDs <sup>[10-11]</sup> are proposed. Upconversion phosphors are materials that emit visible light by irradiating near-infrared rays as excitation light. Therefore, researches in the field of biological functioning, such as bio-imaging <sup>[1-3]</sup> and photodynamic therapy (PDT) <sup>[4-6]</sup>, have often been performed. Further, the emission mechanism has been clear that the upconversion phosphors were researched by F. Auzel <sup>[12-14]</sup>.

As a significant problem in the preparation of fluorescent nanoparticles, a uniform distribution of rare-earth ions in host materials is important. When rare-earth ions are distributed heterogeneously in host materials, self-quenching occurs because of the migrating excitation energy. Because the probability of non-radiative relaxation by a trap state such as a surface defect increases, the luminous efficiency decreases. The uniform distribution of rare-earth ions is a significant theme in the field of nanoparticles <sup>[15, 16]</sup>.

Further, fluorescent nanoparticles have been prepared by various wet chemical methods, such sol-gel method <sup>[17, 18]</sup>, hydrothermal synthesis method <sup>[19, 20]</sup>, and reverse micelle method <sup>[21, 22]</sup>. In general, however, a sintering process is carried out for the

preparation of nanoparticles. In this low-temperature process, the luminous efficiency is degraded because the crystallinity of nanoparticles is low<sup>[15, 23]</sup>. In contrast, at a high temperature, the particle size is increased by necking nanoparticles with each other<sup>[15, 24]</sup>. It is difficult to prepare fine nanoparticles having a high luminous efficiency. Hence, we have focused on laser ablation in water<sup>[25-32]</sup>. This is a technology that nanoparticles are prepared by irradiating a highly crystalline bulk target with a laser. Thus, the preparation of the highly crystalline nanoparticles is possible. As a general mechanism, when a target is irradiated with a laser, plume plasma is generated on the target. Then, nanoparticles are prepared by quenching this plume plasma around a solvent<sup>[33-37]</sup>. Moreover, a shock wave is generated as an opposite reaction. After the quenching of the plume plasma, cavitation bubbles are generated. Therefore, it is known that a high pressure (in the order of a few gigapascals) is generated on the surface of the targets<sup>[38-41]</sup>. The shock wave and the cavitation bubble have a significant effect on the generation of nanoparticles.

Thus far, we have prepared  $\text{Y}_2\text{O}_3:\text{Er}, \text{Yb}$  nanoparticles by laser ablation in water<sup>[42-44]</sup>. As a result, we have discovered that the nanoparticles having a particle size of a few hundred nanometers can be prepared by using a shock wave and cavitation bubbles and that the nanoparticles having a particle size of a few ten nanometers prepared by the

quenching of plume plasma. However, the details of the crystallinity and the distribution of the dopant in nanoparticles prepared by laser ablation in water are not yet known.

In this study, we investigated the crystallinity and the distribution of the dopant in nanoparticles prepared by laser ablation in water. For the preparation of the nanoparticles, nano-second Nd:YAG laser was used. The crystallinity of the nanoparticles was investigated by using an X-ray diffractometer (XRD). The distribution of the dopant in the nanoparticles was investigated by using scanning transmission electron microscopy-energy dispersive X-ray spectroscopy (STEM-EDX). The optical properties of the nanoparticles were investigated by using a photoluminescence spectrophotometer (PL).

## **Experimental section**

### **Synthesis of target**

A target was synthesized by using a general sol-gel method. As a start material,  $\text{Y}(\text{NO}_3)_3 \cdot 6\text{H}_2\text{O}$  (99.99% Kanto Chemical Co., Inc),  $\text{Er}(\text{NO}_3)_3 \cdot 5\text{H}_2\text{O}$  (99.9% Mitsuwa's Pure Chemical),  $\text{Yb}(\text{NO}_3)_3 \cdot n\text{H}_2\text{O}$  (99.99% Kanto Chemical Co., Inc.), and aqueous ammonia (28% Kanto Chemical Co., Inc.) were used.  $\text{Y}(\text{NO}_3)_3 \cdot 6\text{H}_2\text{O}$  (11.1 mmol),  $\text{Er}(\text{NO}_3)_3 \cdot 5\text{H}_2\text{O}$  (0.125 mmol), and  $\text{Yb}(\text{NO}_3)_3 \cdot n\text{H}_2\text{O}$  (1.25 mmol) were dissolved in

de-ionized water. Aqueous ammonia (11 mL) was added to the solution. The prepared solution was aged for 24 h. The precipitations were dried at 60 °C for 24 h. The dried powder was calcined at 900 °C for 2 h. The calcined powder was pressed into shapes and sintered at 1250 °C for 4 h. The target was 9 mm in diameter and 3 mm in height.

### **Laser ablation in water**

The prepared target was placed at the bottom of a plastic cuvette, which was 45 mm in height and 10 mm in length and breath. The plastic cuvette was filled with 2 mL of de-ionized water. The Nd:YAG laser (Spectron Laser Systems Ltd.; SL8585G:wavelength = 532 nm, repetition rate = 10 Hz, and the pulse width = 13 ns) served as a light source for pulsed laser ablation in water. Nanoparticles were prepared by irradiating the targets with the laser.

### **Characterization**

An X-ray diffractometer (XRD, Philips X'pert-PRO-MRD) was used for measuring the crystallinity of the prepared nanoparticles. The prepared  $Y_2O_3:Er,Yb$  nanoparticles were placed onto an elastic carbon supporting film. The film was dried at 60 °C for 1 h. The configuration of the nanoparticles was observed with a scanning electron microscope (SEM, Hitachi High-Technologies Co. S-4800). In the elemental analysis of the nanoparticles, scanning transmission electron microscopy–energy

dispersive X-ray spectroscopy (STEM-EDX, JEOL Ltd. JEM-2100F) was used. Under irradiation with a 980-nm laser diode (LD, THORLABS, Inc. TCLDM9), the upconversion properties of the  $\text{Y}_2\text{O}_3:\text{Er},\text{Yb}$  nanoparticles were measured by using a photoluminescence spectrophotometer (PL, Hitachi High-Technologies Co. F-7000).

## Results and discussion

Figure 1 shows the XRD patterns of the synthesized target and nanoparticles prepared by laser ablation in water. Figures 1(a), (b), and (c) show the XRD patterns of the nanoparticles prepared in the fluence of 1.38, 2.43, 3.61  $\text{J}/\text{cm}^2$ , respectively. Figure 1(d) shows the XRD patterns of the prepared target. It was confirmed that the prepared nanoparticles and the target had  $Ia3$  C-type crystal structure of  $\text{Y}_2\text{O}_3$  (PDF No. 01-089-5592). No additional peak representing any other crystal phase was confirmed in the nanoparticles prepared by laser irradiation. The full-width half-maximum (FWHD) of the peaks at  $2\theta = 29.1^\circ$  was 0.14 in the target. The FWHD of the peaks ( $2\theta = 29.1^\circ$ ) of the nanoparticles prepared by laser ablation in water was between 0.11 and 0.14. Therefore, nanoparticles were prepared by laser ablation in water while maintaining an almost high crystallinity of the target.

Figure 2 shows the SEM images of the nanoparticles after the laser irradiation. Figures 2 (a), (b), (c), and (d) show the SEM images at irradiations times of 5, 15, 30, and 60 min, respectively. The nanoparticles having a particle size of a few tens of nanometers were observed after laser irradiation. These nanoparticles were prepared by quenching the plume plasma generated on the target surface by laser irradiation, because the configuration and the size of the prepared nanoparticles were different from those of the target particles. At irradiation times of between 5 and 15 min, dot-like nanoparticles were observed. In an irradiation time of 30 min, on the other hand, nano-strings, which have a network structure, were observed. In an irradiation time of 60 min, a network structure was generated by aggregating the dot-like nanoparticles. From these results, we concluded that the irradiation time increased with an increase in the number of dot-like nanoparticles. Thereafter, when the irradiation time crossed 30 min, the dot-like nanoparticles aggregated. Nano-strings were generated by heating the aggregated dot-like nanoparticles.

Figure 3 shows the histograms of nanoparticles and nano-strings shown in Figure 2. Figures 3(a) and (b) show the histograms of the particle size of the dot-like nanoparticles at irradiation times of 5 and 15 min, respectively. When the irradiation time was 5 min, the average particle size was  $16.0 \pm 3.7$  nm. In the latter case, the

average particle size was  $18.7 \pm 5.5$  nm. Figures 3(c) and (d) show the histograms of the width of the nano-strings at irradiation times of 30 and 60 min, respectively. In the former case, the average width of the nano-strings was  $21.8 \pm 4.9$  nm. In the latter case, the average width of the nano-strings was  $21.9 \pm 4.9$  nm. From Figures 3(a)–(c), we observed that the irradiation time increased with a gradual increase in the particle size. From Figures 3(c) and (d), we observed that the average width of the nano-strings hardly changed. That is, nano-strings were generated by the aggregation of the dot-like nanoparticles. The structure these nano-strings is known as the network structure prepared by laser ablation in water [45-48]. However, the mechanism of the network structure prepared by laser ablation in water has not yet been clarified. Hence, we investigated why such a network structure was generated by the laser ablation in water. First, dot-like nanoparticles are generated from quenching plume plasma by laser ablation in water. The dot-like nanoparticles are moved randomly by Brownian motion in solution. Second, the number of dot-like nanoparticles increases by additional pulsed laser irradiation. Then, the dot-like nanoparticles collide with each other and neck each other because of the heat generated by the laser irradiation. As a result, nano-strings are generated. That is, Brownian motion is involved in the generation of the abovementioned network structure.

Dot-like nanoparticles generated by quenching plume plasma were investigated in detail by STEM-EDX. Figure 4(a) shows a TEM image of the dot-like nanoparticles. Lattice fringes of the nanoparticles were observed. That is, highly crystalline nanoparticles were observed. Then, lattice constant  $d$  of  $3.06 \text{ \AA}$  were observed. This corresponded to the  $d_{222}$  lattice plane of cubic  $\text{Y}_2\text{O}_3$ . Therefore, it was found that this dot-like nanoparticle was cubic  $\text{Y}_2\text{O}_3$ . Figure 4(b) shows an STEM image of the dot-like nanoparticles. These dot-like nanoparticles were also observed in the TEM image shown in Figure 4(a). Then, a line analysis of the nanoparticles shown in Figure 4(b) was performed using EDX. Figures 4(c), (d), and (e) show the results of this line analysis. The letters in Figure 4(b) correspond to the EDX spectra shown in Figures 4(c), (d), and (e). The results of the EDX analysis revealed the Y ( $\text{K}_\alpha$ ,  $\text{K}_\beta$ ), Er ( $\text{LIII}_{\text{ab}}$ ), and Yb ( $\text{L}_\alpha$ ) peaks. These nanoparticles were generated by quenching the plume plasma prepared by laser irradiation. It was indicated to be recrystallized to  $\text{Y}_2\text{O}_3$ , after the elements changed into the quenched plasma. From results of STEM-EDX, it was found that uniformly Er-Yb-doped  $\text{Y}_2\text{O}_3$  nanoparticles were prepared by laser ablation in water.

Figure 5 shows a bright-field STEM (BF-STEM) image and the EDX mappings of the nanoparticles prepared by laser ablation in water. Further, the aggregation of

nanoparticles having a particle size of a few hundred nanometers was observed. The hydrodynamic diameter measured by dynamic light scattering (DLS) would be almost same as particle size measured by STEM<sup>[49]</sup>. Because the nanoparticles were similar to the configuration and the size of the particles in the target, the nanoparticles depending on these target particles were found<sup>[37]</sup>. The target was fragmented into nanoparticles by the high pressure generated by the shock waves and cavitation bubbles upon laser irradiation. Figure 5(a) shows a BF-STEM image of the nanoparticles prepared by laser ablation in water. Figures 5 (b), (c), (d), and (e) show the STEM-EDX mappings. The EDX mappings of Y ( $K_{\alpha}$ ), Er (LIII<sub>ab</sub>), Yb (L $_{\alpha}$ ), and O ( $K_{\alpha}$ ) were observed. It was found that Er and Yb had a uniform distribution in  $Y_2O_3$ . That is, the activator (Er) and the sensitizer (Yb) were doped in the host materials ( $Y_2O_3$ ).

The mechanism of formation of upconversion nanoparticles by laser ablation in liquid would be classified into two models<sup>[37]</sup>. The first one is related to very fine nanoparticles shown in Figure 4. The irradiation with laser beam to target would generate temperature rise of target and cluster generation and cooling would promote nucleation and particle growth. This mechanism is based on references [35, 36]. The second one is related to coarse nanoparticles shown in Figure 5. The irradiation with laser beam to target generates shock waves. They would cause fragmentation of sintered

target and generate coarse nanoparticles. Particle size and shape of coarse nanoparticle was almost same as those of primary particle of target. Formation mechanism of coarse nanoparticle would be different from that of fine nanoparticle. Figure 6(a) shows the upconversion spectrum of the target upon irradiation with 980 nm LD. The red ( ${}^2F_{9/2} \rightarrow {}^4I_{15/2}$ ) and green ( ${}^2H_{11/2}, {}^4S_{3/2} \rightarrow {}^4I_{15/2}$ ) emissions were observed in the target. It was found that Er and Yb were doped in the Y site of the targets. Therefore, it was clear that the nanoparticles depended on the light emitted by the target particles. However, whether the nanoparticles generated upon the quenching of the plume plasma emitted light or not was not known. We investigated the optical properties of the nanoparticles generated from the quenching of the plume plasma. Then, these nanoparticles were separated from the nanoparticles that depended on the target particles by using a membrane filter (Omnipore membrane filter, Filter Type: 0.1  $\mu\text{m}$  Merck Millipore). The upconversion spectra of the nanoparticles generated by the quenching of the plume plasma were measured under irradiation with 980 nm LD, as well as the target. As a result, red ( ${}^2F_{9/2} \rightarrow {}^4I_{15/2}$ ) and green ( ${}^2H_{11/2}, {}^4S_{3/2} \rightarrow {}^4I_{15/2}$ ) emissions were observed in the nanoparticles generated by quenching the plume plasma, as well as the target (Figure 6(a)). Therefore, on the basis of the optical properties, it was found that the nanoparticles generated by quenching the plume plasma doped Er and Yb in  $\text{Y}_2\text{O}_3$ .

Figure 7 shows the energy-level diagrams of Er and Yb. The emission mechanism was found by F. Auzel <sup>[12-14]</sup>. First, the red emission ( ${}^2F_{9/2} \rightarrow {}^4I_{15/2}$ ) was considered. Upon irradiation with 980 nm LD,  ${}^2F_{7/2} \rightarrow {}^2F_{5/2}$  of Yb and  ${}^4I_{15/2} \rightarrow {}^4I_{11/2}$  of Er were excited. The energy transfer to Er happened because of the relaxation of Yb. Then, non-radiative relaxation of  ${}^4I_{11/2} \rightarrow {}^4I_{13/2}$  occurred in Er.  ${}^4I_{13/2} \rightarrow {}^4F_{9/2}$  of Er was excited by the irradiation with 980 nm LD and the energy transfer of Yb. Thereafter, the red emission happened by backing to the ground state ( ${}^2F_{9/2} \rightarrow {}^4I_{15/2}$ ). Second, the green emission ( ${}^2H_{11/2}, {}^4S_{3/2} \rightarrow {}^4I_{15/2}$ ) was considered. Upon irradiation with 980 nm LD,  ${}^4I_{15/2} \rightarrow {}^4I_{11/2}$  of Er was excited.  ${}^4I_{11/2} \rightarrow {}^4F_{7/2}$  of Er was excited by the irradiation of 980 nm LD and the energy transfer of Yb. The non-radiative relaxation of  ${}^4F_{7/2} \rightarrow {}^2H_{11/2}$  and  ${}^4F_{7/2} \rightarrow {}^4S_{3/2}$  in Er occurred. Then, the green emission occurred due to backing to the ground state ( ${}^2H_{11/2}, {}^4S_{3/2} \rightarrow {}^4I_{15/2}$ ).

Compared to the emission intensity of the target, the emission intensity of nanoparticles was lower than that of the target. In general, the specific surface area of nanoparticles was increased more than that of the bulk. When the specific surface area was increased, the amount of absorption of  $\text{OH}^-$  and  $\text{CO}_3^{2-}$  increased. In particular, it was easy to absorb  $\text{OH}^-$  on the surface of the nanoparticles prepared by laser ablation in water. When molecules with high vibration energy, such as  $\text{OH}^-$  and  $\text{CO}_3^{2-}$ , absorbed on

the surface of the nanoparticles, the thermal relaxation rate increased. As a result, the emission intensity decreased [50].

Figure 8 shows the red emission intensity as a function of the excitation light power (980 nm LD). In both the target and the prepared nanoparticles, the red emission intensity increased with increasing excitation light power. In general, the emission intensity increased next [12, 51].

$$I_{em} \propto P_{ex}^n$$

where  $I_{em}$  denotes the emission intensity;  $P_{ex}$ , the excitation power of a laser diode; and  $n$ , the number of photons. However, the red emission intensity was dramatically increased at an excitation power of 90 mW. Further, this phenomenon was also observed in the case of the green intensity. This effect was called photon avalanche. This mechanism is explained in [52]–[54]. The photon avalanche effect is a phenomenon that occurs in the cross-relaxation section. Figure 9 shows the photon avalanche process. In general, the red intensity is emitted by the absorbance of  ${}^4I_{15/2} \rightarrow {}^4I_{11/2}$  and  ${}^4I_{13/2} \rightarrow {}^4F_{9/2}$  (excited-state absorption: ESA). However, a cross-relaxation section between  ${}^4F_{9/2} \rightarrow {}^4I_{13/2}$  and  ${}^4I_{15/2} \rightarrow {}^4I_{13/2}$  is formed. Then, the electron population in the  ${}^4I_{13/2}$  band is increased by the formation of the cross relaxation section and the non-radiative relaxation of  ${}^4I_{11/2} \rightarrow {}^4I_{13/2}$ . The excitation of  ${}^4I_{13/2} \rightarrow {}^4F_{9/2}$  occurs upon irradiation with

980 nm LD. As a result, red light is emitted by  ${}^4F_{5/2} \rightarrow {}^4I_{15/2}$ . Therefore, an increase in this electron population causes a dramatic increase in the emission intensity. From these results, it was found that the optical properties of the prepared nanoparticles exhibited the same optical properties as those of the target particles.

## **Conclusions**

$Y_2O_3:Er,Yb$  nanoparticles were successfully prepared by laser ablation in water, while maintaining the high crystallinity of the target. At various irradiation times, it was found that nano-strings were generated within 30 min. In the TEM image, lattice fringes of the nanoparticles were observed. Further, highly crystalline nanoparticles were observed. When a line analysis of the nanoparticles was carried out by STEM-EDX, Y ( $K_\alpha, K_\beta$ ), Er ( $L_{IIIab}$ ), and Yb ( $L_\alpha$ ) peaks were observed. In the PL spectrum of the nanoparticles, the red emission ( ${}^2F_{9/2} \rightarrow {}^4I_{15/2}$ ) and the green emission ( ${}^2H_{11/2}, {}^4S_{3/2} \rightarrow {}^4I_{15/2}$ ) were confirmed, as well as the targets. The prepared nanoparticles exhibited a photon avalanche effect. On the basis of these results, it was confirmed that uniformly Er-Yb-doped  $Y_2O_3$  nanoparticles were prepared by laser ablation in water.

## **Acknowledgments**

These works were carried out in Materials and Structure Laboratory (Tokyo Institute of Technology) as collaborative research. We would like to express our sincere gratitude to Prof. Kazutaka Nakamura (laser equipment) of Tokyo Tech and Mr. Hiroshi Iida (XRD measurement) and Mr. Naoyuki Hatakeyama (STEM-EDX measurement) of Center for Advanced Materials Analysis, Tokyo Tech.

## References

- [1] Jing Zhou, Zhuang Liub and Fuyou Li, *Chemical Society Review*, (2012) 41, 31323
- [2] Masao Kamimura, Daisuke Miyamoto, Yu Saito, Kohei Soga, and Yukio Nagasaki, *Langmuir*, (2008), 24, 8864
- [3] S. F. Lim, R. Riehn, W. S. Ryu. N. Khanarian, C. Tung, D. Tank, R, H, Austin, *Nano Letters*, 6 (2006) 169.
- [4] Hai Sheng Qian, Hui Chen Guo, Paul Chi-Lui Ho, Ratha Mahendran, and Yong Zhang, *Small*, 5 (2009) 2285
- [5] Jingning Shan, Stephanie J. Budijono, Guohong Hu, Nan Yao, Yibin Kang, Yiguang Ju, and Robert K. Prud'homme, *Advanced Functional Materials*, 21 (2011) 2488
- [6] Chao Wang, Huiquan Tao, Liang Cheng, and Zhuang Liu, *Biomaterials*, 32 (2011) 6145
- [7] Bryan M. van der Ende, Linda Aartsa, and Andries Meijerink, *Physical Chemistry Chemical Physics*, 11 (2009) 11081
- [8] Jefferson Luis Ferrari, Karmel de Oliveira Lima,<sup>a</sup> Edison Pecoraro, Rute A. S. Ferreira, Luís D. Carlos, and Rogéria Rocha Gonçalves, *Journal of Materials Chemistry*, 22 (2012) 9901

- [9] Shi Chen, Guohong Zhou, Fenfang Su, Hailong Zhang, Liangxing Wang, Mengjia Wu, Mingbo Chen, Likun Pan, Shiwei Wang, *Materials Letters*, 77 (2012) 17
- [10] S. Ye, F. Xiao, Y. X. Pan, Y. Y. Ma, and Q. Y. Zhang : *Materials Science and Engineering R*, 71 (2010) 1
- [11] Naoto Hirotsuki, Rong-Jun Xie, Koji Kimoto, Takashi Sekiguchi, Yoshinobu Yamamoto, Takayuki Suehiro, and Mamoru Mitomo, *Applied Physics Letters*, 86 (2005) 211905
- [12] F. Auzel., *Chemical Reviews* 104 (2004) 139
- [13] F. Auzel, *F. C. R. Acad. Sci. (Paris)* 262 (1966) 1016
- [14] F. Auzel, *F.C.R. Acad. Sci. (Paris)* 263B (1966) 819
- [15] I. Yu, T. Isobe, and M. Senta, *Journal of Physics and Chemistry of Solids* 54 (1996) 373
- [16] J. G. Li, X. D. Li, X. Sun, and T. Ishigaki *Journal of Physical Chemistry C* 112 (2008) 11707
- [17] Basak Yazgan Kokuoz, Karn Serivalsatit, Baris Kokuoz, Olt Geiculescu, Exley McCormick, and John Ballatow: *Journal of American Ceramics Society*, 92 (2009)

[18] James A. Dorman, Ju H. Choi, Gregory Kuzmanich, and Jane P. Chang: *Journal of Physical Chemistry C*, 116 (2012) 10333

[19] Xia Li, Qiang Li, Jiyang Wang, and Jing Li: *Journal of Luminescence*, 124 (2007) 351

[20] Sreerenjini Chandra, Francis Leonard Deepak, John B. Gruber, and Dhiraj K. Sardar: *Journal of Physical Chemistry C*, 114 (2010) 874

[21] Takayuki Hirai, Yoko Asada, Isao Komasa: *Journal of Colloid and Interface Science*, 276 (2004) 339

[22] Olivia A. Graeve, Jessica O. Corral: *Optical Materials*, 29 (2006) 24

[23] H. M. H. Fadlalla, C. C. Tang, E. M. Elssfah, and F. Shi, *Materials Chemistry and Physics* 109 (2008) 436

[24] J. G. Li, X. D. Li, X. Sun, T. Ikegami, and T. Ishigaki, *Chemistry of Materials* 20 (2008) 2274-2281

[25] Neddersen, J.; Chumanov, G.; Cotton, T. M. *Appl. Spectrosc.* **1993**, *47*, 1959.

[26] G. W. Yang, J. B. Wang, Q. X. Liu, *J. Phys.: Condens. Matter* 10 (1998) 7923.

- [27] Mafuné, F.; Kohno, J.; Takeda, Y.; Kondow, T.; Sawabe, H. *J. Phys. Chem. B* **2000**, 104, 9111.
- [28] J. B. Wang, G. W. Yang, C. Y. Zhang, X. L. Zhong, ZH. A. Ren, *Chem. Phys. Lett.* 367 (2003) 10.
- [29] G. W. Yang, *Prog. Mater. Sci.* 52 (2007) 648.
- [30] P. Liu, Y. L. Cao, C. X. Wang, X. Y. Chen, G. W. Yang, *Nano Lett.* 8 (2008) 2570.
- [31] P. Liu, H. Cui, C. X. Wang, G. W. Yang, *Phys. Chem. Chem. Phys.* 12 (2010) 3942.
- [32] Sajti, C, L.; Sattari, R.; Chichkov, B, N.; Barcikowski, S. *J. Phys. Chem. C* **2010**, 114, 2421.
- [33] Koji Hatanaka, Mitsushi Kawao, Yasuyuki Tsuboi, Hiroshi Fukumura, and Hiroshi Masuhara: *Journal of Applied Physics*, 82 (1997) 11
- [34] Tetsuo Sakka, Kazuhiro Takatani, Yukio H Ogata and Mahito Mabuchi: *Journal of Physics D: Applied Physics*, 35 (2002) 65
- [35] C. X. Wang, P. Liu, H. Cui, G. W. Yang, *Appl. Phys. Lett.* 87 (2005) 201913.
- [36] G. W. Yang: *Laser Ablation in Liquids: Principles and Applications in the Preparation of Nanomaterials* (Pan Stanford publishing, 2012) Chap. 3.
- [37] Vincenzo Amendola and Moreno Meneghetti: *Physcal Chemistry Chemical Physics*, 15 (2013) 3027

- [38] R. Fabbro, J. Fournier, P. Ballard, D. Devaux, and J. Virmont: *Journal of Applied Physics*, 68 (1990) 775
- [39] L. Berthe, R. Fabbro, P. Peyre, L. Tollier, and E. Bartnick: *Journal of Applied Physics*, 82 (1997) 2826
- [40] L. Berthe, R. Fabbro, P. Peyre, E. Bartnick: *Journal of Applied Physics*, 85 (1999) 7552
- [41] L. Berthe, A. Sollier, P. Peyre, R. Fabbro and E. Bartnicki: *Journal of Physics D: Applied Physics*, 33 (2000) 2142
- [42] Takashi Nunokawa, Yuji Onodera, Masahiko Hara, Yoshitaka Kitamoto, Osamu Odawara, and Hiroyuki Wada: *Applied Surface Science*, 261 (2012) 118
- [43] Yuji Onodera, Takashi Nunokawa, Osamu Odawara, and Hiroyuki Wada: *Journal of Luminescence*, 137 (2013) 220
- [44] Takashi Nunokawa, Yuji Onodera, Hikaru Kobayashi, Tsuyoshi Asahi, Osamu Odawara and Hiroyuki Wada: *Journal of Ceramic Processing Research*, 14 (2013) s1
- [45] Ken-ichi Saitow, Yoshinori Okamoto, and Yohko F. Yano: *Journal of Physical Chemistry C*, 116 (2012) 17252
- [46] S. Besner, A. V. Kabashin and M. Meunier: *Applied Physics A*, 88, (2007) 269

- [47] Jean-Philippe Sylvestre, Suzie Poulin, Andrei V. Kabashin, Edward Sacher, Michel Meunier, and John H. T. Luong: *Journal of Physical Chemistry B*, 108 (2004) 16864
- [48] Takeshi Tsuji, Norihis Watanabe, and Masaharu Tsuji: *Applied Surface Science*, 211 (2003) 189
- [49] T. Nunokawa, Y. Onodera, M. Hara, Y. Kitamoto, O. Odawara, H. Wada, *Appl. Surf. Sci.* 261 (2012) 118.
- [50] Fiorenzo Vetrone, John-Christopher Boyer, John A. Capobianco, Adolfo Speghini, and Marco Bettinelli: *Chemistry of Materials*, 15 (2003) 2737
- [51] F. Auzel: *Journal of Luminescence*, 31-32 (1984) 759
- [52] Jay S. Chivian, W. E. Case, and D. D. Eden: *Applied Physics Letters*, 35 (1979) 124
- [53] M. F. Joubert, S. Guy, and B. Jacquie: *Physical Review B*, 48 (1993) 10031
- [54] Marie. F. Joubert: *Optical Materials* 11 (1999) 181

## Figures

**Figure 1.** XRD patterns of the nanoparticles prepared in the fluence of 1.38 (a), 2.43 (b), 3.61 J/cm<sup>2</sup> (c), and the synthesized targets (d).

**Figure 2.** SEM images of the nanoparticles prepared by the laser irradiation. Irradiation times were 5 (a), 15 (b), 30 (c), and 60 min (d).

**Figure 3.** Histograms of nanoparticles and nano-strings shown in Figure 2.

**Figure 4.** TEM image of the dot-like nanoparticles (a), STEM image of the dot-like nanoparticles (b), and line analysis of the dot-like nanoparticles by EDX (c), (d), and (e).

**Figure 5.** BF-STEM image and EDX mappings of the nanoparticles prepared by laser ablation in water: BF-STEM image (a), Y mapping (b), Er mapping (c), Yb mapping (d), and O mapping (e).

**Figure 6.** Upconversion spectra of the target (a) and nanoparticles (b) upon irradiation with 980 nm LD.

**Figure 7.** Energy-level diagrams of Er<sup>3+</sup> and Yb<sup>3+</sup> in Y<sub>2</sub>O<sub>3</sub> upon irradiation with 980 nm

LD.

**Figure 8.** Red emission intensity (660 nm) as a function of the excitation power of 980 nm LD: target (a) and nanoparticles (b).

**Figure 9.** General photon avalanche process of energy-level diagram of  $\text{Er}^{3+}$  ions in  $\text{Y}_2\text{O}_3$ .

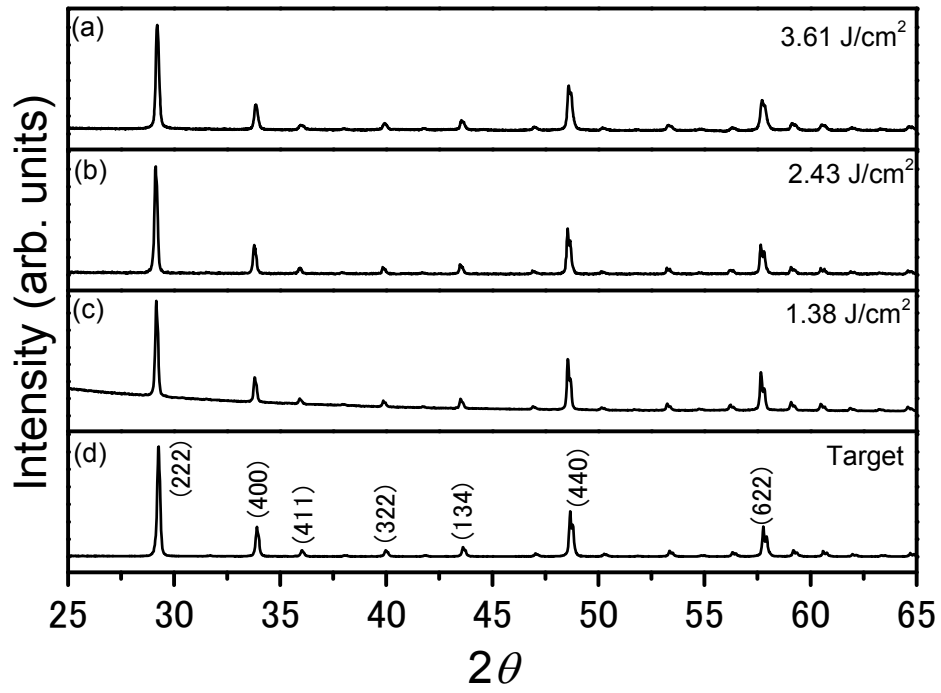


**Figure 1.** XRD patterns of the nanoparticles prepared in the fluence of 1.38 (a), 2.43 (b), 3.61 J/cm<sup>2</sup> (c), and the synthesized targets (d).

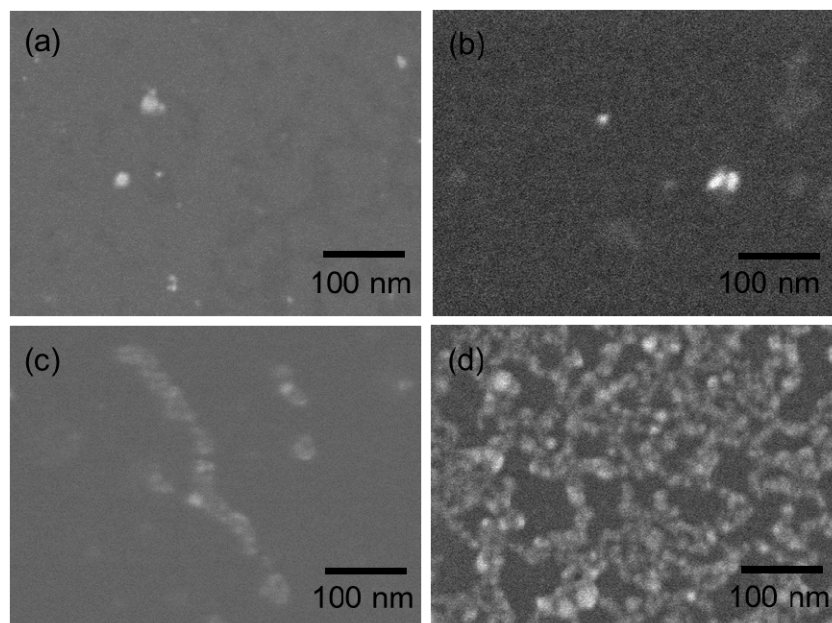


**Figure 2.** SEM images of the nanoparticles prepared by the laser irradiation. Irradiation times were 5 (a), 15 (b), 30 (c), and 60 min (d).

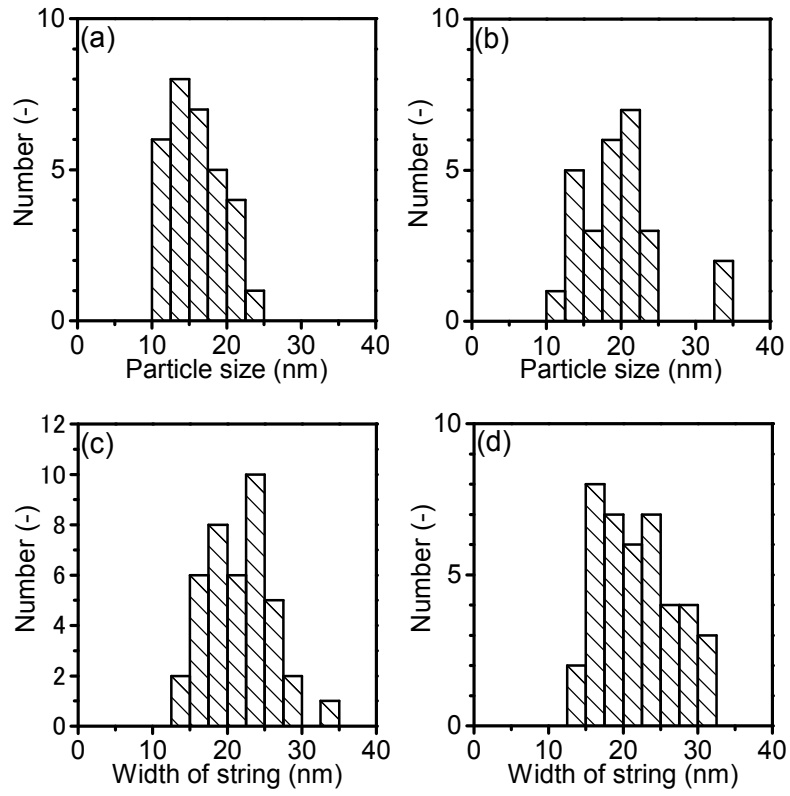


**Figure 3.** Histograms of nanoparticles and nano-strings shown in Figure 2.

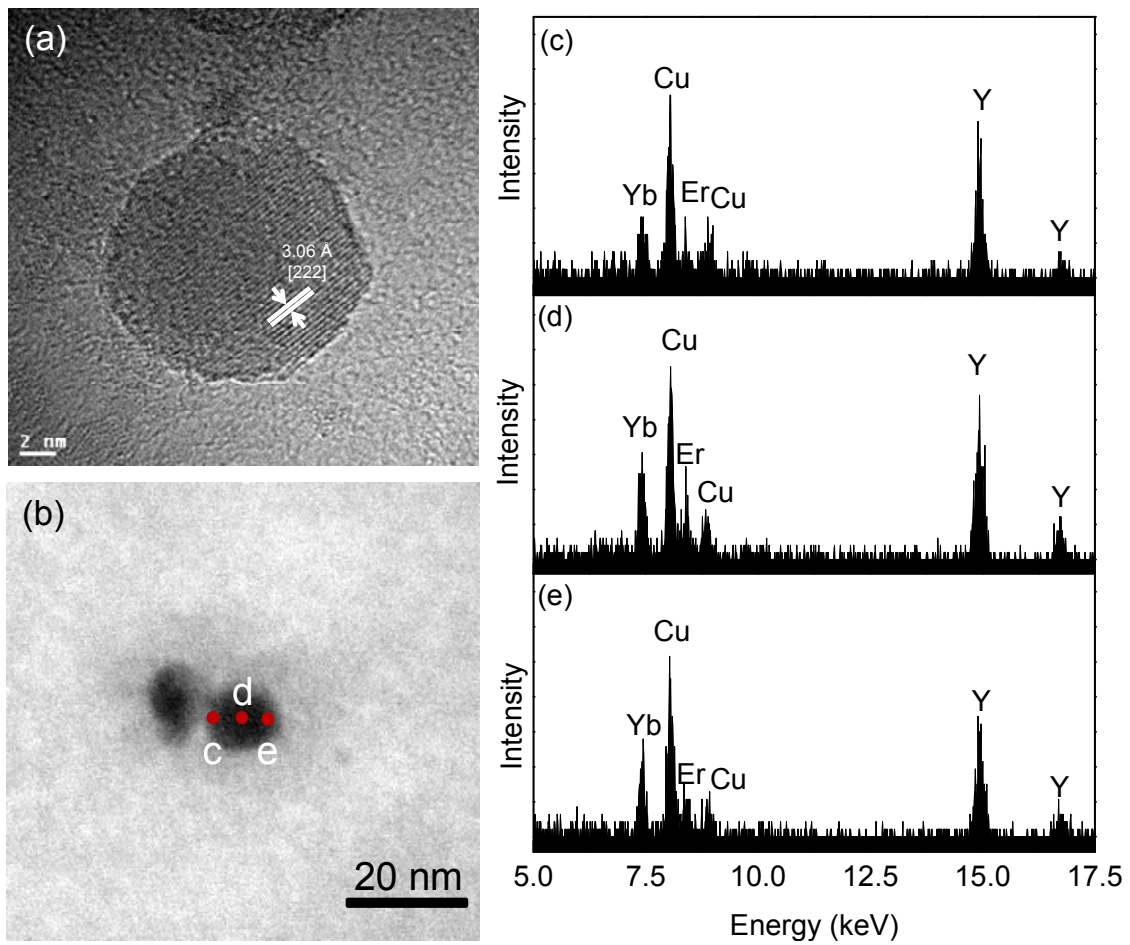


**Figure 4.** TEM image of the dot-like nanoparticles (a), STEM image of the dot-like nanoparticles (b), and line analysis of the dot-like nanoparticles by EDX (c), (d), and (e).

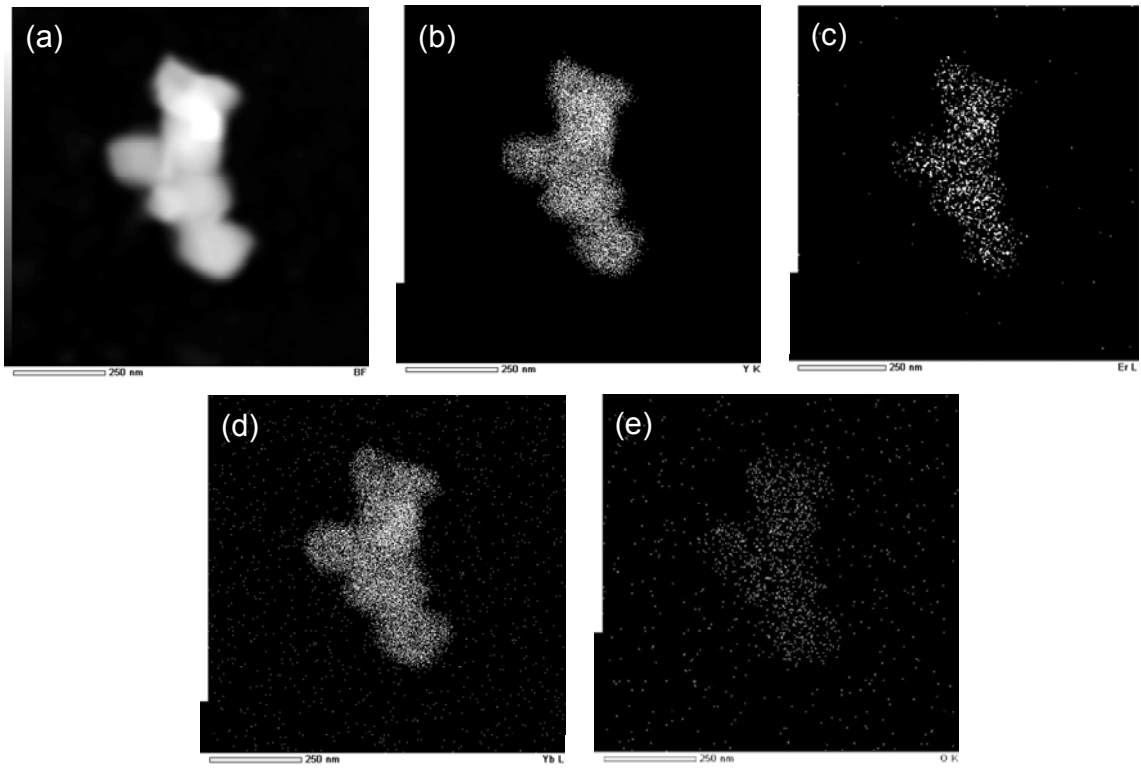


**Figure 5.** BF-STEM image and EDX mappings of the nanoparticles prepared by laser ablation in water: BF-STEM image (a), Y mapping (b), Er mapping (c), Yb mapping (d), and O mapping (e).

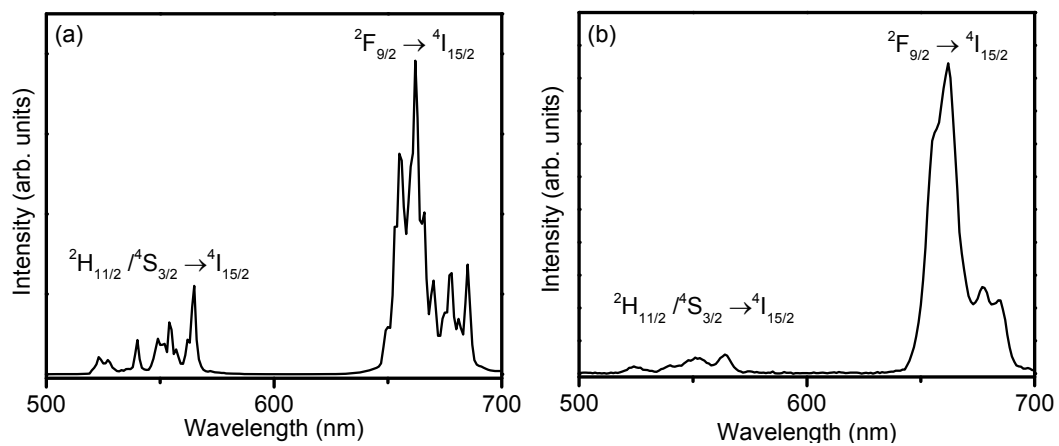


**Figure 6.** Upconversion spectra of the target (a) and nanoparticles (b) upon irradiation with 980 nm LD.

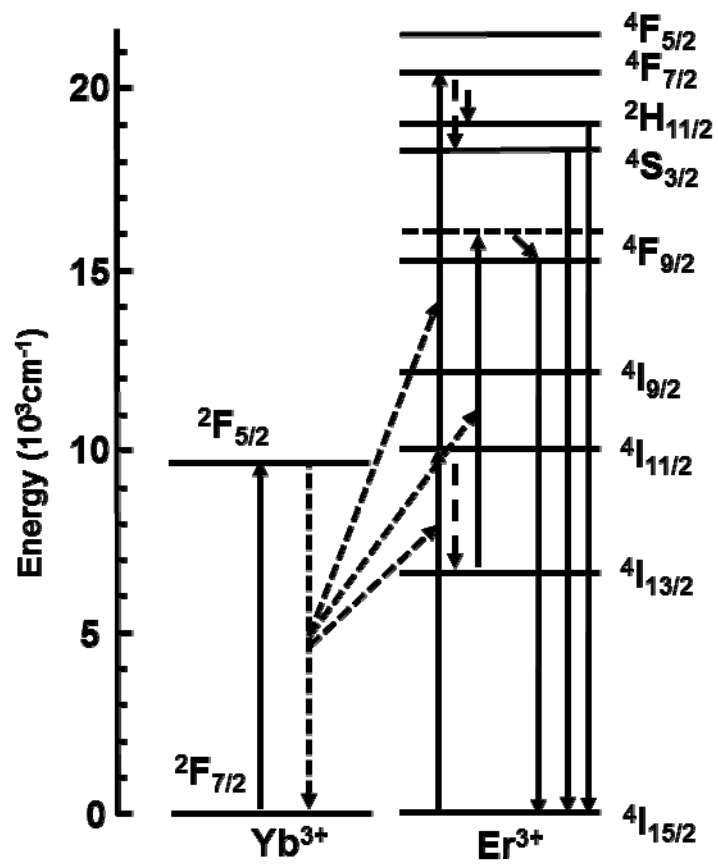


**Figure 7.** Energy-level diagrams of Er<sup>3+</sup> and Yb<sup>3+</sup> in Y<sub>2</sub>O<sub>3</sub> upon irradiation with 980 nm

LD.

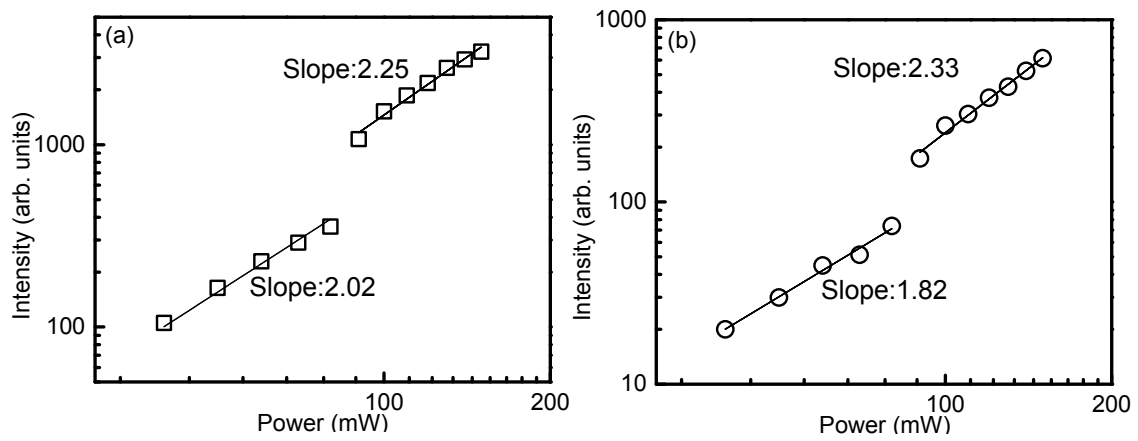


**Figure 8.** Red emission intensity (660 nm) as a function of the excitation power of 980 nm LD: target (a) and nanoparticles (b).

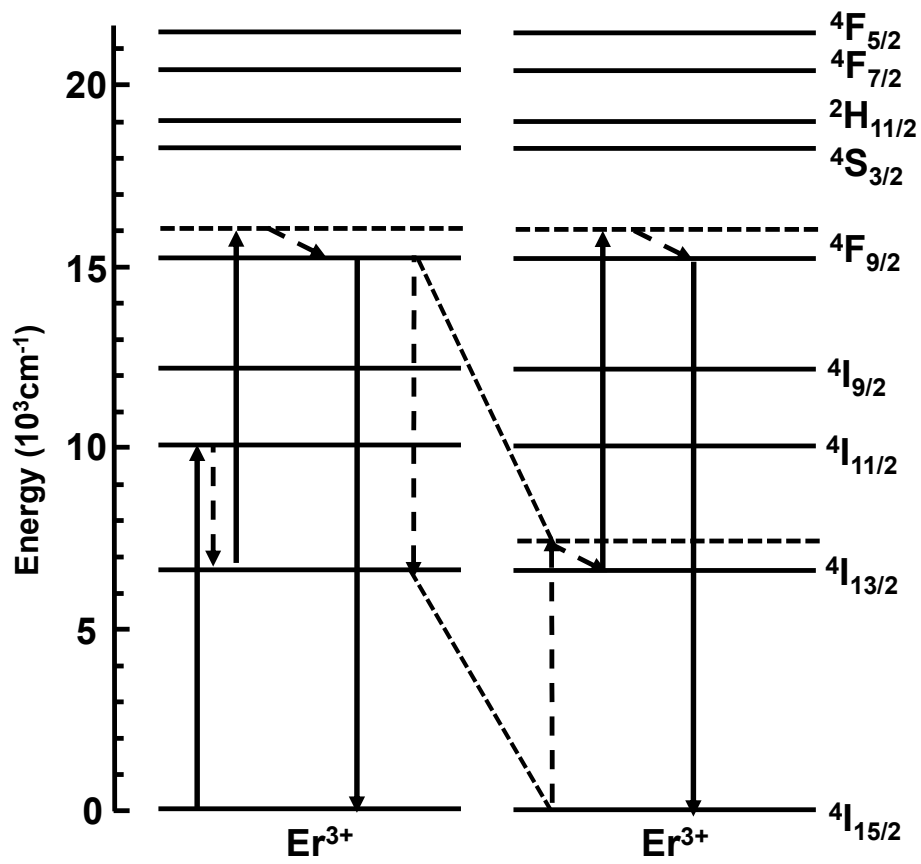


**Figure 9.** General photon avalanche process of energy-level diagram of  $\text{Er}^{3+}$  ions in

$\text{Y}_2\text{O}_3$ .